Tomography and weak lensing statistics

Journal of Cosmology and Astroparticle Physics
An IOP and SISSA journal

Tomography and weak lensing statistics

Dipak Munshi,[a,b] **Peter Coles**[a,b] **and Martin Kilbinger**[c,d,e]

[a]Astronomy Centre, School of Mathematical and Physical Sciences, University of Sussex, Department of Physics and Astronomy, Brighton, BN1 9QH U.K.
[b]School of Physics & Astronomy, Cardiff University, 5 The Parade, Cardiff, CF24 3AA U.K.
[c]Excellence Cluster Universe, Boltzmannstrasse 2, Garching bei München, D-85748 Germany
[d]Universitäts-Sternwarte München, Scheinerstr. 1, München, 81679 Germany
[e]CEA Saclay, Service d'Astrophysique (SAp), Orme des Merisiers, Bat 709, F-91191 Gif-sur-Yvette

E-mail: D.Munshi@sussex.ac.uk, peter.coles@astro.cf.ac.uk, martin.kilbinger@cea.fr

Received September 4, 2012
Revised January 21, 2014
Accepted March 18, 2014
Published April 2, 2014

Abstract. We provide generic predictions for the lower order cumulants of weak lensing maps, and their correlators for tomographic bins as well as in three dimensions (3D). Using small-angle approximation, we derive the corresponding one- and two-point probability distribution function for the tomographic maps from different bins and for 3D convergence maps. The modelling of weak lensing statistics is obtained by adopting a detailed prescription for the underlying density contrast that involves *hierarchal ansatz* and lognormal distribution. We study the dependence of our results on cosmological parameters and source distributions corresponding to the realistic surveys such as LSST and DES. We briefly outline how photometric redshift information can be incorporated in our results. We also show how *topological* properties of convergence maps can be quantified using our results.

Keywords: weak gravitational lensing, dark matter theory, dark energy theory

ArXiv ePrint: 1112.0495

doi:10.1088/1475-7516/2014/04/004

JCAP04(2014)004

Contents

JCAP04(2014)004

1 Introduction

Following the first weak lensing measurements [3, 24, 51, 58], the field of weak lensing has witnessed a tremendous progress in all fronts (see [32] for a review). In terms of cosmological observations, weak lensing surveys, such as the CFHT[1] legacy survey, the Pan-STARRS,[2] the Dark Energy survey (DES),[3] the Large Synoptic Survey Telescope (LSST)[4] and Joint Dark Energy Mission or JDEM[5] will play a role complementary to both Cosmic Microwave Background (CMB) studies and studies involving large scale structure (LSS) surveys.

In this paper we extend previous results [22, 30, 31, 33, 54] on projected surveys by analysing the entire one-point PDF and the two-point PDF with tomographic information. All previous results were derived for pro 2D or projected surveys.

The PDF contains information about the correlation hierarchy to an arbitrary order; the correlation hierarchy of the convergence field is directly related to that of the underlying mass distribution. We employ a generating function formalism that relies on *hierarchical ansatz* (HA) on smaller angular scales and on perturbative results on larger scales. We

[1] http://www.cfht.hawaii.edu/Science/CFHLS/.
[2] http://pan-starrs.ifa.hawaii.edu/public/.
[3] https://www.darkenergysurvey.org/.
[4] http://www.lsst.org/lsst/.
[5] http://jdem.gsfc.nasa.gov/.

define a reduced convergence for each bin and show that the different bins sample the same underlying PDF and bias functions (to be defined later) for the density contrast. The entire joint two-point PDFs for different pairs of redshift bins and individual PDFs for each bins can be constructed from the PDFs and the bias associated with individual bins because the joint PDF is factorisable in terms of the individual PDFs, bias and cross-correlations among various bins and different angular scales. We generalise these tomographic results to entire 3D convergence using small-angle approximation.

Though these results are derived using HA, they will have wider applicability, as they are independent of details of HA. Other well motivated approximations for PDF such as the lognormal distribution can also be used along with these results (see e.g. [18, 19, 21] for various aspects of lognormal distribution). Our results will have relevance for *Gaussianization* of weak-lensing statistics [59, 60]. We consider models involving dark energy [1, 55] to check sensitivity of different parametrization.

This paper is organised as follows. In section 2 we introduce our notation and present some standard results. In section 3 we link the lower order statistics of weak lensing convergence to that of the underlying density distribution. In section 4 we briefly review the HA in the context of generating function formalism which is summarised in section 5. In section 6 we discuss the lognormal model in the context of weak lensing statistics. In section 7 we derive the PDF and bias for various tomographic bins. The results are quite generic and can be used for arbitrary source redshift distribution. We extend these results to 3D in section 8. Effect of noise is discussed in section 9. Finally the section 10 is left for discussion of our results.

In A we outline how Minkowski functionals can be used to quantify topological properties of convergence maps.

2 Notation

The statistics of the weak lensing convergence $\kappa(\hat{\Omega})$ represents that of the projected density contrast $\delta(\mathbf{x})$ along the line of sight. In our analysis we will consider a small patch of the sky where we can use the plane parallel approximation or small angle approximation to replace the spherical harmonics by Fourier modes. The 3-dimensional density contrast δ along the line of sight when projected onto the sky with the weight function $\omega(r)$ gives the weak lensing convergence in a direction $\hat{\Omega}$ which we have denoted by $\kappa(\hat{\Omega})$. For a distribution of sources represented by $p_s(z)$ we can write the projected convergence $\kappa(\hat{\Omega})$ as follows:

$$\kappa(\hat{\Omega}) = \int_0^{r_{\rm H}} dr\ \omega(r)\ \delta(r,\hat{\Omega}); \qquad \kappa^{\rm min} = -\int_0^{r_{\rm H}} dr\ \omega(r); \tag{2.1}$$

$$\omega(r) = \frac{3}{2}\frac{H_0^2}{c^2}\Omega_{\rm M} a^{-1}(r)\frac{1}{\bar{n}_g}\ d_A(r)\ \int_r^{r_{\rm H}} dr_s\ p_s(z)\frac{dz}{dr_s}\frac{d_A(r-r_s)}{d_A(r_s)}; \tag{2.2}$$

$$p_s(z) = \bar{n}_g \frac{z^2}{2z_0^3}\exp(-z/z_0). \tag{2.3}$$

We have assumed a flat Universe. The comoving radial distance is denoted as r at a redshift z i.e. in terms of Hubble paramter H(z): $r = \int_0^z dz'/H(z')$; $d_A(r)$ denotes comoving angular diameter distance. H_0 is the Hubble parameter, c speed of light, and $a = (1+z)^{-1}$ represents the scale factor at a redshift z. The survey parameters z_0 (median survey redshift $= 2z_0$) and $\bar{n}_g = \int_0^\infty dr_s p_s(z)(dz/dr_s)$ (average surface density of galaxies) will be specified below.

JCAP04(2014)004

In a tomographic analysis the source population is divided into several redshift bins and each of which is treated separately. The convergence $\kappa_{(i)}(\hat{\Omega})$ from i-th tomographic bin can be expressed as:

$$\text{Tomography}: \quad \kappa_{(i)}(\hat{\Omega}) = \int_0^{r_{\rm H}} dr\; w_{(i)}(r)\; \delta[r, \hat{\Omega}]; \tag{2.4}$$

$$w_{(i)}(r) = \frac{3}{2}\frac{H_0^2}{c^2}\Omega_{\rm M}\frac{1}{\bar{n}_i}a^{-1}(r)\; d_A(r) \int_{\max\{r,r_i\}}^{r_{i+1}} dr_s\; p_s(z)\frac{dz}{dr_s}\frac{d_A(r-r_s)}{d_A(r_s)}. \tag{2.5}$$

The "bin average" of the source population is denoted by $\bar{n}_i$ and is defined accordingly $\bar{n}_i = \int_{r_i}^{r_{i+1}} dr_s p_s(z)(dz/dr_s)$. We will consider different bin sizes and source distributions. To incorporate the photometric redshift error we can write

$$\text{Photometric Redshift Errors}: \quad w_{(i)}^{\rm photo}(r) = \frac{3}{2}\frac{H_0^2}{c^2}\Omega_{\rm M}\frac{1}{\bar{n}_i}a^{-1}(r)d_A(r)\int_{\max\{r,r_i\}}^{r_{i+1}} dr' \left[\sum_h p_h(z'|z_h)\right]\frac{d_A(r-r')}{d_A(r')}. \tag{2.6}$$

The probability distribution p_h signifies posterior probability distribution of redshift given a photometric redshift of z_h. In our calculation we will need to define a new variable $\kappa^{\rm min}$ (or $\kappa^{\rm min}_{(i)}$ for tomographic bins) which will be useful later:

$$\kappa^{\rm min}_{(i)} = \int_0^{r_{\rm H}} dr\; w_{(i)}(r); \tag{2.7}$$

In evaluation of $\kappa^{\rm min}_{(i)}$ we use the following approximate form for the window $w_i(r)$:

$$w_{(i)}(r) \approx \Delta r_s \frac{3}{2}\frac{H_0^2}{c^2}\Omega_{\rm M}\; a^{-1}\; \frac{1}{\bar{n}_i}\; d_A(r)\; p_s(z(r_i))\left[\frac{dz}{dr_s}\right]_{r=r_i}\frac{d_A(r_i-r)}{d_A(r_i)}. \tag{2.8}$$

We will adopt two example survey configurations to make definitive calculation. For DES we will take $z_0 = 0.3$ and for LSST we will take $z_0 = 0.4$. The range of source distribution that we consider for each survey is $z_s = 0.2 - 1.6$. The bin-size we take is $\Delta z_s = 0.2$. The constant $\bar{n}_g$ is set by imposing the normalized condition $\int_0^\infty\; dz\; p_s(z) = 1$. For our purpose we have $\bar{n}_g = 1.2 \times 10^7 \bar{n}'_g$ (n_g specifies the galaxy number density per square arc-minutes). We will vary n_g from few galaxies per arcmin^2 to tens of galaxies per arcmin^2. The noise power spectrum $C_\ell^{\rm N}$ in terms of the intrinsic ellipticity $\gamma_i^2 = 0.1$ is expressed as $C_\ell^{\rm N} = \gamma_i^2/\bar{n}_g$.

The particular ΛCDM cosmology that we will adopt as a baseline for our numerical study is specified by the following parameter values: $\Omega_\Lambda = 0.741, h = 0.72, \Omega_b = 0.044, \Omega_{\rm CDM} = 0.215, \Omega_{\rm M} = \Omega_b + \Omega_{\rm CDM}, n_s = 0.964, w_0 = -1, w_a = 0, \sigma_8 = 0.803, \Omega_\nu = 0$. We will consider two different dark energy equation (DE) of state [57]: (i) constant equation of state $w_0 = -0.95$; and (ii) with evolving equation of state $w_{\rm X}(z) = -1 + z/(1+z)$ and compare against ΛCDM predictions while keeping all other parameters fixed.

In figure 1 we plot the parameter $\kappa_{\rm min}$ as a function of redshift for different cosmologies (left panel). We also show the number distribution of source galaxies (right panel). We notice that $|\kappa^{\rm min}|$ is higher for ΛCDM compared to the two DE models we have considered for the range of redshift we have considered.

JCAP04(2014)004

3 Lower order statistics of tomographic convergence maps

Using these definitions we can compute the projected two-point correlation function in terms of the dark matter power spectrum $P_\delta(k,r)$ [23, 45]:

$$\langle\kappa_{(i)}(\hat{\Omega}_1)\kappa_{(j)}(\hat{\Omega}_2)\rangle_c = \int_0^{r_{\rm H}} dr \frac{\omega_{(i)}(r)\omega_{(j)}(r)}{d_A^2(r)} \int \frac{d^2\mathbf{l}}{(2\pi)^2}\ \exp(i\theta_{12}\cdot\mathbf{l})\ \mathrm{P}_\delta\left[\frac{\ell}{d_A(r)};r\right] W_{\rm TH}^2(\ell\theta_0). \tag{3.1}$$

Here θ_{12} is the angular separation projected onto the surface of the sky ($\cos|\theta_{12}| = \hat{\Omega}_1\cdot\hat{\Omega}_2$) and we have also introduced $\mathbf{l} = d_A(r)\mathbf{k}_\perp$ to denote the scaled projected wave vector; $\omega_{(i)}(r)$ are the weak lensing projection weights for the ith tomographic bins defined in eq. (2.5); to include photometric redshift errors we simply need to use $\omega_{(i)}^{\rm photo}(r)$ defined in eq. (2.6). Using Limber's approximation [28] the variance of $\kappa_{(i)}(\theta_0)$ smoothed using a top-hat window $W_{\rm TH}(\theta_0)$ with a radius θ_0 can be written as:

$$\langle\kappa_{(i)}^2\rangle = \int_0^{r_{\rm H}} dr \frac{\omega_{(i)}^2(r)}{d_A^2(r)} \int \frac{d^2\mathbf{l}}{(2\pi)^2}\ \mathrm{P}_\delta\Big(\frac{\ell}{d_{\rm A}(r)};r\Big) W_{\rm TH}^2(\ell\theta_0). \tag{3.2}$$

The variance is plotted for different redshift bins in figure 2. Similarly the higher order moments of the smoothed convergence field relate $\langle\kappa^p(\theta_0)\rangle$ to the 3-dimensional (3D) multi-spectra of the underlying dark matter distribution B_p [34]

$$\begin{aligned}\langle\kappa_{(i)}^p\rangle_c = &\int_0^{r_{\rm H}} dr \frac{\omega_{(i)}^p(r)}{d_{\rm A}^{2(p-1)}(r)} \int \frac{d^2\mathbf{l}_1}{(2\pi)^2}\mathrm{W}_{\rm TH}(\ell_1\theta_0)\cdots\int\frac{d^2\mathbf{l}_p}{(2\pi)^2}\mathrm{W}_{\rm TH}(\ell_p\theta_0)\\ &\times\mathrm{B}_p^\delta\Big(\frac{\ell_1}{d_A(r)},\cdots,\frac{\ell_p}{d_{\rm A}(r)};r\Big)_{\sum\mathbf{l}_i=0}.\end{aligned} \tag{3.3}$$

The subscripts $\sum\mathbf{l}_i = 0$ represent the delta function $\delta_{\rm D}(\sum\mathbf{l}_i)$. The higher order cumulant correlators of the smoothed convergence field relating $\langle\kappa_{(i)}^p(\hat{\Omega}_1)\kappa_{(j)}^q(\hat{\Omega}_2)\rangle_c$ with multi-spectra of underlying dark matter distribution B_{p+q}^δ can similarly be expressed as [34, 35, 48]:

$$\begin{aligned}\langle\kappa_{(i)}^p(\hat{\Omega}_1)\kappa_{(j)}^q(\hat{\Omega}_2)\rangle_c = &\int_0^{r_{\rm H}}\frac{\omega_{(i)}^p(r)\omega_{(j)}^q(r)}{d_{\rm A}^{2(p+q-1)}(r)}dr\\ &\times\int\frac{d^2\mathbf{l}_1}{(2\pi)^2}\cdots\int\frac{d^2\mathbf{l}_{p+q}}{(2\pi)^2}\mathrm{W}_{\rm TH}(\ell_1\theta_0)\cdots\mathrm{W}_{\rm TH}(\ell_{p+q}\theta_0)\\ &\times\exp(i\theta_{12}\cdot\mathbf{l}_{p+q})\mathrm{B}_{p+q}^\delta\left(\frac{\ell_1}{d_{\rm A}(r)},\frac{\ell_2}{d_{\rm A}(r)},\cdots,\frac{\ell_{p+q}}{d_{\rm A}(r)};r\right)_{\sum\mathbf{l}_i=0}.\end{aligned} \tag{3.4}$$

We will use and extend these results in this paper to show that it is possible to compute the whole bias function $b(>\kappa)$, i.e. the bias associated with those spots in convergence map which κ is above certain threshold (which acts as a generating function for these cumulant correlators) from the statistics of underlying over-dense dark objects [37, 38].

The results presented here are generalisation of our previous studies where only projected surveys were considered.

JCAP04(2014)004

4 Hierarchical *ansatze*

The spatial length scales corresponding to small angles are in the highly non-linear regime of gravitational clustering. Assuming a "minimal tree" model for the matter correlation hierarchy in the highly non-linear regime, one can write the general form of the pth order correlation function $\xi_\delta^{(p)}$ as [2, 4, 5, 45, 47] In general for correlation functions of arbitrary order are constructed by taking a sum over all possible *topologies* with respective amplitudes parameters $Q_{N,\alpha}$, which in general will be different:

$$\xi_\delta^{(\mathrm{p})}(\mathbf{r}_1,\dots\mathbf{r}_\mathrm{p}) = \sum_{\alpha,\mathrm{p-trees}} Q_{p,\alpha} \sum_{\text{labellings}} \prod_{\text{edges}}^{(\mathrm{p}-1)} \xi_\delta^{(2)}(\mathbf{r}_i,\mathbf{r}_j)\,. \tag{4.1}$$

We will use $\xi_\delta^{(2)}(r_1,r_2) \equiv \xi_{12}$ and $\bar{\xi}_2$ for its volume average over a volume v. In Fourier space such an ansatz means that the hierarchy of multi-spectra can be written as sums of products of the matter power-spectrum: In general for p-the order poly-spectra $B_\delta^{(p)}(\mathbf{k_1},\dots\mathbf{k_p})$ we can write:

$$\mathrm{B}_\delta^{(\mathrm{p})}(\mathbf{k}_1,\dots\mathbf{k}_\mathrm{p}) = \sum_{\alpha,\mathrm{p-trees}} Q_{\mathrm{p},\alpha} \sum_{\text{labellings}} \prod_{\text{edges}}^{(p-1)} P_\delta(\mathbf{k}_i,\mathbf{k}_j)\,. \tag{4.2}$$

Different hierarchical models differ in the way they predict the amplitudes of different tree topologies [6, 7, 37–39, 47]. We express the one-point cumulants as:

$$\langle\kappa^3_{(i)}\rangle_c = (3Q_3)\mathcal{C}_3^{(i)}[\kappa^2_{\theta_0}] = S_3^{(i)}\langle\kappa^2_{(i)}\rangle_c^2 \tag{4.3}$$

$$\langle\kappa^4_{(i)}\rangle_c = (12R_a+4R_b)\mathcal{C}_4^{(i)}[\kappa^3_{\theta_0}] = S_4^{(i)}\langle\kappa^2_{(i)}\rangle_c^3\,, \tag{4.4}$$

where we have introduced the following notation:

$$\mathcal{C}_p^{(i)}\Big[[\mathcal{J}_{\theta_0}(r)]^{p-1}\Big] = \int_0^{r_s} \frac{\omega^p_{(i)}(r)}{d_A^{2(p-1)}(r)}[\mathcal{J}_{\theta_0}(r)]^{p-1}dr\,; \tag{4.5}$$

$$[\mathcal{J}_{\theta_0}(r)] \equiv \int \frac{d^2\mathbf{l}}{(2\pi)^2} P_\delta\left(\frac{\ell}{d_\mathrm{A}(r)}\right) \mathrm{W}^2_{\mathrm{TH}}(l\theta_0)\,. \tag{4.6}$$

The normalised cumulants for convergence in the i-th bin are denoted by (skewness) $S_3^{(i)}$ and (kurtosis) $S_4^{(i)}$. The two-point statistics such as the cumulant correlators [33, 34] for individual bins are expresses as follows:

$$\begin{aligned}\langle\kappa^2_{(i)}(\hat{\Omega}_1)\kappa_{(j)}(\hat{\Omega}_2)\rangle_c &= 2Q_3\mathcal{C}_3^{(ij)}[\mathcal{J}_{\theta_0}(r)\mathcal{J}_{\theta_{12}}(r)] \\ &= C_{21}^\eta\mathcal{C}_3^{(ij)}[\mathcal{J}_{\theta_0}(r)\mathcal{J}_{\theta_{12}}(r)] \equiv C_{21}^{(ij)}\langle\kappa^2_{(i)}\rangle_c\langle\kappa_{(i)}(\hat{\Omega}_1)\kappa_{(j)}(\hat{\Omega}_2)\rangle_c\,,\end{aligned} \tag{4.7}$$

$$\begin{aligned}\langle\kappa^3_{(i)}(\hat{\Omega}_1)\kappa_{(j)}(\hat{\Omega}_2)\rangle_c &= (3R_a+6R_b)\mathcal{C}_4^{(ij)}[\mathcal{J}_{\theta_0}(r)\mathcal{J}_{\theta_{12}}(r)] \\ &= C_{31}^\eta\mathcal{C}_4^{(ij)}[\mathcal{J}_{\theta_0}(r)^2\mathcal{J}_{\theta_{12}}(r)] \equiv C_{(31)}^{(ij)}\langle\kappa^2_{(i)}\rangle_c^2\langle\kappa_{(i)}(\hat{\Omega}_1)\kappa_j(\hat{\Omega}_2)\rangle_c\,.\end{aligned} \tag{4.8}$$

Where we have introduced the following notation:

$$\mathcal{C}_{p+q}^{(ij)}\Big[[\mathcal{J}_{\theta_0}(r)]^{p+q-2}[\mathcal{J}_{\theta_{12}}(r)]\Big] = \int_0^{r_s} \frac{\omega^p_{(i)}(r)\omega^q_{(j)}(r)}{d_A^{2(p+q-1)}(r)}[\mathcal{J}_{\theta_0}(r)]^{p+q-2}[\mathcal{J}_{\theta_{12}}(r)]dr\,; \tag{4.9}$$

$$[\mathcal{J}_{\theta_{12}}(r)] \equiv \int \frac{d^2\mathbf{l}}{(2\pi)^2} P_\delta\left(\frac{\ell}{d_\mathrm{A}(r)}\right) \mathrm{W}^2_{\mathrm{TH}}(\ell\theta_0)\exp(\mathbf{l}\cdot\boldsymbol{\theta_{12}})\,. \tag{4.10}$$

JCAP04(2014)004

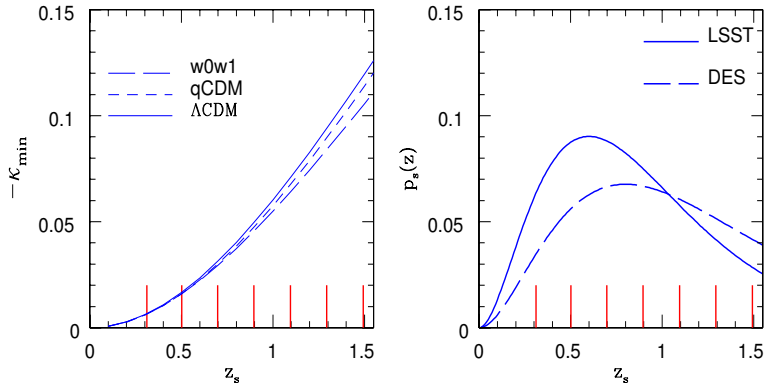

Figure 1. The parameter $\kappa_{\rm min}$ is plotted as a function of redshift z_s in the left panel for various background cosmologies. The right panel shows the source density distribution (not normalised) for the two different surveys. The lines along the x-axis denotes the positions of the tomographic bins considered in our analysis. Notice that the parameter $k_{\rm min}$ do not depend on smoothing angular scales and only depend on the depth of the survey as well as on redshift distribution of source population. We consider two different dark energy models along with ΛCDM cosmology. The curve qCDM correspond to $w_0 = -0.95$ and the model w0w1 correspond to an evolving dark energy model $w(z) = -1 + z/(1 + z)$.

where C^{η}_{pq} denotes the cumulant correlators for the underlying mass distribution. These results essentially employ the small angle approximation or Limber's approximation [28] that are routinely used in computation of higher order cumulants in many cosmological contexts. Other approximations such as the Born approximation that we use have been verified by testing against simulations. It is important to note that our results generalise previous results by using tomographic bins.

In figure 2 we have plotted the variance and the lower order S_p parameters respectively as a function of smoothing scale θ_0.

5 The generating function and probability distribution functions

In a scaling analysis the generating function of one-point cumulants or S_p parameters: $\phi(y) = \sum_{p=1}^{\infty} S^{\delta}_p/p!y^p$ plays a crucial role in construction of a PDF [2, 56]. The function $\phi(y)$ satisfies the constraint $S^{\delta}_1 = S^{\delta}_2 = 1$ necessary for proper normalization of PDF. The other generating function which plays a very important role in such analysis is the generating function for the vertex amplitudes ν_n associated with nodes appearing in the tree representation of higher order correlation hierarchy ($Q_3 = \nu_2$, $R_a = \nu_2^2$ and $R_b = \nu_3$). In practice it is possible to work with a perturbative expansion of the vertex generating function $\mathcal{G}(\tau)$. In terms of the vertices this is defined as: $\mathcal{G}(\tau) = \sum_{n=0}^{\infty}(-1)^n\nu_n/n!$. However in the highly nonlinear regime a closed form is used. A more specific model for $\mathcal{G}(\tau)$, which is useful to make more specific predictions [2, 5] is given by $\mathcal{G}(\tau) = \left(1 + \tau/\kappa_a\right)^{-\kappa_a}$. We will relate κ_a with other parameters of scaling models. While the definition of VPF does not involve any specific form of hierarchical *ansatz* it is to realize that writing the tree amplitudes in terms of the weights associated with nodes is only possible when one assumes a factorisable model of the tree hierarchy [5] and other possibilities which do not violate the tree models are indeed possible too [9]. The generating functions for tree nodes can be related to the $\phi(y)$ by solving a pair

JCAP04(2014)004

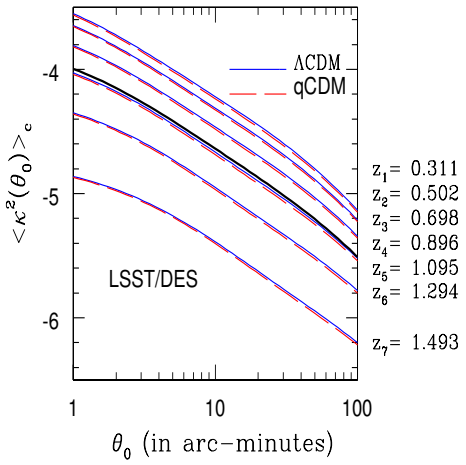

Figure 2. The plots shows the variance in convergence $\langle\kappa^2(\theta_0)\rangle_c$ as a function of smoothing angular scales θ_0. A top-hat window has been assumed. The curves from top to bottom correspond to various tomographic bins. The redshift bins correspond to $\Delta z_s = 0.2$ and covers a range $z_s = 0.2 - 1.4$.The curve qCDM correspond to $w_0 = -0.95$. The higher curves correspond to the deeper redshift bins. See text for more details.

of implicit equations [2],

$$\phi(y) = y\mathcal{G}(\tau) - \frac{1}{2}y\tau\frac{d}{d\tau}\mathcal{G}(\tau)\,; \qquad \tau = -y\frac{d}{d\tau}\mathcal{G}(\tau)\,. \tag{5.1}$$

The above description has been limited to the level of constructing one-point PDF. A more detailed analysis is needed to include the effect of correlation between two or more correlated volume element which will provide information about bias and cumulant correlators. The bias $b(\delta)$ can be introduced the following expression for the joint or two-point PDF:

$$p(\delta_1, \delta_2)d\delta_1 d\delta_2 = p(\delta_1)p(\delta_2)(1 + b(\delta_1)\xi_{12}b(\delta_2))d\delta_1 d\delta_2 \tag{5.2}$$

The function $\tau(y)$ - sometimes denoted by $\beta(y)$ in the literature - plays the role of a generating function for the factorized cumulant correlators C^η_{p1} ($C^\eta_{pq} = C^\eta_{p1}C^\eta_{q1}$) [2, 6, 7, 9]: $\tau(y) = \sum_{p=1}^{\infty} y^p C^\eta_{p1}/p!$. We will next consider two different regimes; the quasilinear regime valid at large angular scales and the highly nonlinear regime valid at smaller angular scales.

The PDF $p(\delta)$ and bias $b(\delta)$ can be related to generating functions $\phi(y)$ and $\tau(y)$ respectively by following equations [2, 6, 9]

$$p(\delta) = \int_{-i\infty}^{i\infty}\frac{dy}{2\pi i}\exp\left[\frac{(1+\delta)y - \phi(y)}{\bar{\xi}_2}\right]; \tag{5.3}$$

$$b(\delta)p(\delta) = \int_{-i\infty}^{i\infty}\frac{dy}{2\pi i}\tau(y)\exp\left[\frac{(1+\delta)y - \phi(y)}{\bar{\xi}_2}\right]. \tag{5.4}$$

It is worth mentioning that, there have been various attempts to extend the perturbative results to the highly nonlinear regime (see e.g. [17, 40]).

6 The lognormal distribution

An alternative to the hierarchical ansatz, the *lognormal* distribution, for the description of the matter PDF which has long been known as a successful empirical prescription for

JCAP04(2014)004

the characterization of the dark matter distribution as well as the observed galaxy distribution [12, 15, 27]. Detailed discussion for comparison of lognormal distribution and the perturbative calculations can be found in [8]. The lognormal distribution was further generalized to the *skewed*-lognormal distribution [16]. In general a variable might be modelled as lognormal if it can be thought of as the multiplicative product of many independent random variables.

Although inherently local in nature, the lognormal distribution can provide a good fit to both one-point PDF and its generalisation to compute its two-point analog and hence the bias [49]. The one- and two-point lognormal PDF can be expressed as [25]:

$$p_{\rm ln}(\delta)d\delta = \frac{1}{\sqrt{2\pi\bar{\Sigma}}}\exp\left[-\frac{\Delta^2}{2\Sigma^2}\right]\frac{d\delta}{1+\delta}\,; \tag{6.1}$$

$$\Sigma^2 = \ln(1+\sigma^2)\,; \qquad \Delta = \ln\left[(1+\delta)\sqrt{(1+\sigma^2)}\right]\,; \tag{6.2}$$

$$p_{\rm ln}(\delta_1,\delta_2)d\delta_1 d\delta_2 = \frac{1}{2\pi\sqrt{\Sigma^2-X_{12}^2}}\exp\left[-\frac{\Sigma(\Delta_1^2+\Delta_2^2)-2X_{12}\Delta_1\Delta_2}{2(\Sigma^2-X_{12}^2)}\right]\frac{d\delta_1}{1+\delta_1}\frac{d\delta_2}{1+\delta_2}\,; \tag{6.3}$$

$$\Delta_i = \ln\left[(1+\delta_i)\sqrt{(1+\bar{\xi}_2^2)}\right]\,; \qquad \Sigma_{12} = \ln(1+\xi_{12}) \tag{6.4}$$

In the limiting case of large separation $X_{12} \to 0$ we can write down the two point PDF

$$p_{\rm ln}(\delta_1,\delta_2) = p_{\rm ln}(\delta_1)p_{\rm ln}(\delta_2)[1+b_{\rm ln}(\delta_1)\xi_{12}b_{\rm ln}(\delta_2)]\,; \qquad b_{\rm ln}(\delta_i) = \Delta_i/\Sigma_i\,. \tag{6.5}$$

It is however easier to estimate the cumulative or integrated bias associated with objects beyond a certain density threshold δ_0. This is defined as $b_{\rm ln}(\delta > \delta_0) = \int_{\delta_0}^{\infty} p_{\rm ln}(\delta)b_{\rm ln}(\delta)d\delta / \int_{\delta_0}^{\infty} p_{\rm ln}(\delta)d\delta$. In the low variance limit $\bar{\xi}_2 \to 0$ the usual Gaussian result is restored $b(\delta) = \delta/\bar{\xi}_2$. The parameters $\Lambda, \Lambda_i, X_{12}, \Sigma$ that we have introduced above can be expressed in terms of the two-point (non-linear) correlation function $\xi_{12} = \langle\delta_1\delta_2\rangle$ and the nonlinear variance $\sigma^2 = \langle\delta^2\rangle$ of the smoothed density field. The hierarchical model with a generating function $\mathcal{G}(\tau) = \exp(-\tau)$ can be shown to be equivalent to lognormal distribution. This leads to the following skewness and kurtosis parameters:

$$S_3^\eta = 3+\sigma^2; \qquad S_4^\eta = 16+15\sigma^2+6\sigma^4+\sigma^6. \tag{6.6}$$

In general the $\sigma^2 \to 0$ leads to $S_p^\eta = p^{p-2}$.

7 The PDF and bias of tomographic convergence maps

For computing the probability distribution function of the smoothed convergence field for individual tomographic maps $\kappa^{(i)}(\theta_0)$, we will begin by constructing its associated cumulant generating function for individual tomographic bins $\Phi^{(i)}_{1+\kappa(\theta_0)}(y)$. The construction is based on modelling of the volume-averaged higher order correlation function $\langle\kappa^p_{(i)}(\theta_0)\rangle_c$ in terms of the matter correlation hierarchy:

$$\Phi^{(i)}_{1+\kappa(\theta_0)}(y) = y + \sum_{p=2}^{\infty}\frac{\langle\kappa^p_{(i)}(\theta_0)\rangle_c}{\langle\kappa^2_{(i)}(\theta_0)\rangle_c^{p-1}}y^p. \tag{7.1}$$

JCAP04(2014)004

Now using the expressions for the higher moments of the convergence $\kappa(\theta_0)$ in terms of the matter power spectrum, eq. (3.2) and eq. (4.3) we can relate $\Phi^{(i)}_{1+\kappa_{\theta_0}}$ and ϕ:

$$\Phi^{(i)}_{1+\kappa_{\theta_0}}(y) = \int_0^{r_s} dr \left[\frac{d_A^2(r)\bar{\xi}_2^{(i)\kappa}(\theta_0)}{\mathcal{J}_{\theta_0}(r)}\right] \phi \left[\frac{\omega_{(i)}(r)}{d_A^2(r)} \frac{\mathcal{J}_{\theta_0}(r)}{\bar{\xi}_2^{(i)\kappa}(\theta_0)} y\right] - y\kappa^{\rm min}_{(i)}. \tag{7.2}$$

We will define a new reduced convergence field $\eta_{(i)}(\theta_0)$:

$$\eta_{(i)}(\theta_0) = (\kappa^{\rm min}_{(i)} - \kappa_{(i)}(\theta_0))/\kappa^{\rm min}_{(i)} = 1 + \kappa_{(i)}(\theta_0)/|\kappa^{\rm min}_{(i)}|\,. \tag{7.3}$$

The cumulant generating function of η, i.e. $\Phi^{(i)}_\eta(y)$ is given by,

$$\Phi^{(i)}_\eta(y) = \frac{1}{[\kappa^{\rm min}_{(i)}]} \int_0^{r_s} dr \left[\frac{d_A^2(r)}{\kappa^{\rm min}_{(i)}} \frac{\bar{\xi}_2^{(i)\kappa}(\theta_0)}{\mathcal{J}_{\theta_0}(r)}\right] \phi \left[\omega_{(i)}(r) \frac{\kappa^{\rm min}_{(i)}}{d_A^2(r)} \frac{\mathcal{J}_{\theta_0}(r)}{\bar{\xi}_2^{(i)\kappa}(\theta_0)} y\right]. \tag{7.4}$$

The thus constructed cumulant generating function $\Phi_\eta(y)$ satisfies the normalization constraints $S^\eta_1 = S^\eta_2 = 1$. The scaling function associated with $p(\eta)$ can now be easily related with the matter scaling function $h(x)$ introduced earlier:

$$h^{(i)}_\eta(x) = -\int_{-i\infty}^{+i\infty} \frac{dy}{2\pi i} \exp(xy)\Phi^{(i)}_\eta(y)\,; \tag{7.5}$$

$$h^{(i)}_\eta(x) = \frac{1}{[\kappa^{\rm min}_{(i)}]} \int_0^{r_s} dr \left[\frac{\bar{\xi}_2^{(i)\kappa}(\theta_0)}{\omega_{(i)}(r)\mathcal{J}_{\theta_0}(r)\kappa^{\rm min}_{(i)}}\right]^2 h\left(\frac{\bar{\xi}_2^{(i)\kappa}(\theta_0)x}{\omega_{(i)}(r)\mathcal{J}_{\theta_0}(r)\kappa^{\rm min}_{(i)}}\right). \tag{7.6}$$

Finally, following procedure detailed in [31], for projected 2D surveys, we can express the the PDF for the smoothed convergence $\kappa(\theta_0)$, interms of the PDF of the reduced convergence $\eta(\theta_0)$, for *individual bins*:

$$p_{(i)}(\kappa) = p_\eta(\eta^{(i)})/|\kappa^{\rm min}_{(i)}|\,. \tag{7.7}$$

This is one of the most important results in this paper.

In figure 3 we show the PDF of the reduced convergence η for smoothing angular scale $\theta_0 = 5'$ for the lognormal and hierarchical approximation discussed above, for individual redshift bins as well as for a projected survey.

7.1 The bias associated with convergence maps

To compute the bias associated with the peaks in the smoothed convergence κ field we have to first develop an analytic expression for the generating field $\beta_\kappa(y_1, y_2)$ for the convergence field $\kappa(\theta_0)$. We will avoid displaying the smoothing angular scale θ_0 for brevity. Throughout the statistics are for smoothed convergence fields. For that we will use the usual definition for the two-point cumulant correlator C_{pq} for the convergence field (for a complete treatment see Munshi & Coles, 1999b):

$$C^{(ij)}_{pq} = \langle \kappa_{(i)}(\hat{\Omega}_1)^p \kappa_{(j)}(\hat{\Omega}_2)^q \rangle_c \Big/ [\bar{\xi}^{(i)}_2]^{p-1} [\bar{\xi}^{(j)}_2]^{q-1} \xi^{(ij)}_{12}\,. \tag{7.8}$$

We will show that, like its density field counterpart the two-point generating function for the convergence field κ can be expressed (under certain simplifying assumptions) as a product

JCAP04(2014)004

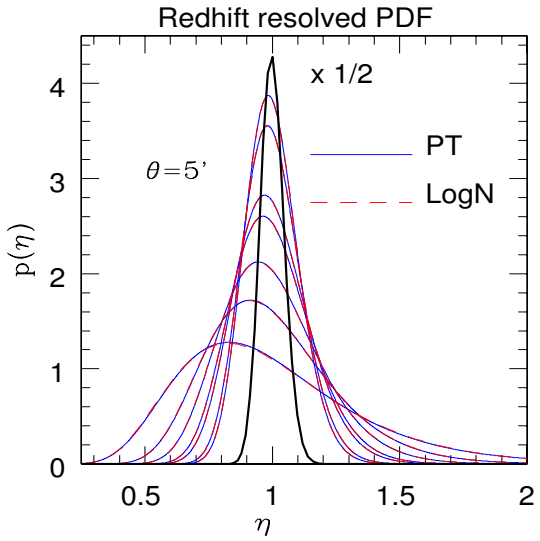

Figure 3. The PDF $p(\eta)$ of the *reduced* convergence η as a function $\eta = 1 + \delta$. The plots with decreasing peak height correspond to lower redshift bins. Two different approximations are being compared. The solid line correspond to the lognormal approximation and the dashed line correspond to the perturbative calculations. The results are shown for a smoothing angular scale $\theta_s = 5'$.

of two one-point generating functions $\beta(y)$ which can then be directly related to the bias associated with "hot-spots"in the convergence field.

$$\begin{aligned}\beta_\eta^{(ij)}(y_1, y_2) &= \sum_{p,q}^{\infty} \frac{C_{pq}^{\eta(ij)}}{p!q!} y_1^p y_2^q = \sum_{p}^{\infty} \frac{C_{p1}^{\eta(i)}}{p!} y_1^p \sum_{q}^{\infty} \frac{C_{q1}^{\eta(j)}}{q!} y_2^q \\ &= \beta_\eta^{(i)}(y_1)\beta_\eta^{(j)}(y_2)\,. \end{aligned} \tag{7.9}$$

The above expression is quite general within the small approximation and large separation approximations, and is valid for any given specific model for the generating function $\mathcal{G}_\delta(\tau)$. However it is easy to notice that the projection effects as encoded in the line of sight integration do not allow us to write down the two-point generating function $\beta_\kappa(y_1, y_2)$ simply as a product of two one-point generating functions $\beta_\eta(y)$ as was the case for the density field $1+\delta$.

$$\begin{aligned}\beta_\kappa^{(ij)}(y_1, y_2) = \int_0^{r_s} d_A^2(r) \frac{1}{\kappa_{(i)}^{\rm min}} \frac{1}{\kappa_{(j)}^{\rm min}} \frac{\mathcal{J}(\theta_{12})}{\bar{\xi}_{12}^{(ij)}} \frac{\bar{\xi}^{(i)}}{\mathcal{J}_{\theta_0}(r)} \frac{\bar{\xi}^{(j)}}{\mathcal{J}_{\theta_0}(r)} \\ \times \beta_\eta^{(i)\kappa}\left(\frac{y_1}{[\bar{\xi}_2^{(i)\kappa}]} \frac{\omega_{(i)}(r)}{d_A^2(r)} \mathcal{J}_{\theta_0}(r)|\kappa_{(i)}^{\rm min}|\right) \beta_\eta^{(j)}\left(\frac{y_2}{[\bar{\xi}_2^{(j)\kappa}]} \frac{\omega_{(j)}(r)}{d_A^2(r)} \mathcal{J}_{\theta_0}(r)|\kappa_{(j)}^{\rm min}|\right).\end{aligned} \tag{7.10}$$

Use of these approximations gives us the leading order contributions to these integrals and we can check that to this order we recover the factorization property of the generating function i.e. $\beta_\eta^{(ij)}(y_1, y_2) = \beta_\eta^{(i)}(y_1)\beta_\eta^{(j)}(y_2) = \beta_{1+\delta}^{(i)}(y_1)\beta_{1+\delta}^{(j)}(y_2)$. So it is clear that at this level of approximation, due to the factorization property of the cumulant correlators, the bias function $b_\eta(x)$ associated with the peaks in the convergence field κ, beyond certain threshold, possesses a similar factorization property too as its density field counterpart. Earlier studies

JCAP04(2014)004

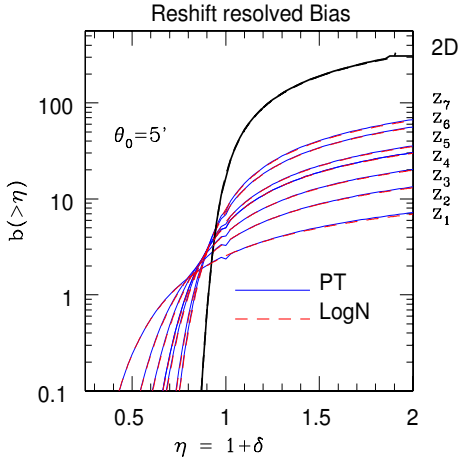

Figure 4. The cumulative bias $b(>\eta)$ of the *reduced* convergence $\eta = (1+\delta)$ is plotted as a function η for various redshift bins. The smoothing angular scale is $\theta_0 = 5'$. As before two different approximations are considered. The lognormal approximation (solid lines) and the perturbative calculations (dashed lines) reproduce nearly identical results. The curves that saturates at a higher values of cumulative bias for higher values of η correspond to larger smoothing angular scales.

have established such a correspondence between convergence field and density field in the case of one-point probability distribution function $p(\delta)$ [30, 31, 33, 44],

$$b_\eta^{(i)}(x_1)h_\eta^{(i)}(x_1)b_\eta^{(i)}(x_2)h_\eta^{(j)}(x_2) = b_{1+\delta}^{(i)}(x_1)h_{1+\delta}^{(i)}(x_1)b_{1+\delta}^{(j)}(x_2)h_{1+\delta}^{(j)}(x_2)\,, \tag{7.11}$$

where we have used the following relation between $\beta_\eta(y)$ and $b_\eta(x)$. The cumulative bias $b_\eta(>x)$ can be defined interms of the generating function $\tau(y)$:

$$b_\eta^{(i)}(x)h_\eta^{(i)}(x) = -\frac{1}{2\pi i}\int_{-i\infty}^{i\infty} dy\; \tau^{(i)}(y)\exp(xy)\,; \tag{7.12}$$

$$b_\eta^{(i)}(>x)h_\eta^{(i)}(>x) = -\frac{1}{2\pi i}\int_{-i\infty}^{i\infty} dy\; \frac{\tau^{(i)}(y)}{y}\exp(xy)\,. \tag{7.13}$$

It is important to notice that, although the bias $b(x)$ associated with the convergence field κ and the underlying density field are identical, the variance associated with the density field is very high, while projection effects substantially reduce the variance in the convergence field. Using eq. (7.7) that $p^{(i)}(\kappa) = p_\eta(\eta)/|\kappa_{\rm min}^{(i)}|$ we also notice that $\xi_{12}^{(ij)} = \xi_{12}^{\eta}/[\kappa_{\rm min}^{(i)}][\kappa_{\rm min}^{(j)}]$, from which we can now write:

$$b_{(i)}(\kappa) = b_\eta^{(i)}(\eta)/|\kappa_{(i)}^{\rm min}|\,. \tag{7.14}$$

Together with eq. (7.7), eq. (7.14) can be used to construct analytical estimates of pdf and bias about individual bins. In addition these results are applicable to the modelling of joint PDFs involving two separate redshift bins.

Figure 4 shows the bias associated with the reduced convergence for individual bins as well as for the entire survey. The smoothing angular scale is $\theta_0 = 5'$. In figure 5 shows the PDF and bias associated with the convergence κ. In figure 6 we plot the difference in PDF between various cosmological scenarios.

JCAP04(2014)004

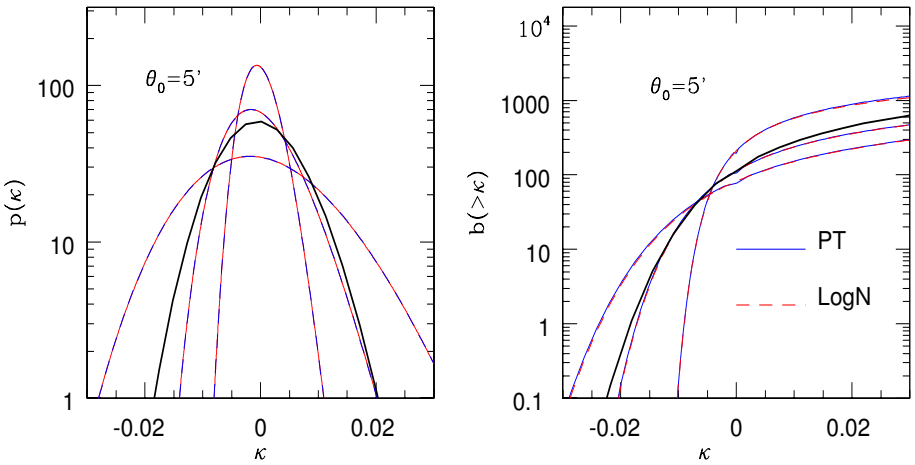

Figure 5. The left panel shows the PDF of the redshift resolved convergence and the right panel shows the associated cumulative bias. The smoothing angular scales considered is $\theta_0 = 5'$. Only three tomographic bins are chosen for display to avoid cluttering. Two different approximations are used; the lognormal distribution and the perturbative calculations. The approximations give near identical results. Three different redshift bins are displayed $z_s = 0.698, 1.095, 1.493$ (top,middle and bottom curve respectively).

8 The PDF and bias for 3D convergence

In this section we will generalise the results obtained in section 7 for tomographic bins to 3D convergence using plane-parallel approximation. The 3D lensing has been studied in great detail in the context of power-spectrum analysis [13, 26, 42, 43] (see [26] for more discussion on use of the plane-parallel approximation in 3D studies of weak-lensing convergence in the context of harmonic analysis). The 3D weak lensing convergence $\kappa(\mathbf{r})$ in plane parallel (Limber) approximation can be expressed in terms of the density contrast δ as:

$$\kappa(\mathbf{r}) \equiv \kappa(r, \hat{\Omega}) = \int_0^r dr' w_{3D}(r, r')\, \delta(r', \hat{\Omega})\,; \tag{8.1}$$

$$\Omega_{3D}(r, r') \equiv \frac{3}{2}\frac{H_0}{c^2}\Omega_M\, a^{-1}\, \frac{r'(r-r')}{r}\,. \tag{8.2}$$

We will also need the minimum value of κ as a function r i.e. $\kappa_m(r)$ this is a generalisation of $\kappa_m^{(i)}$ previously introduced:

$$\kappa_m(r) = -\int_0^r w_{3D}(r, r')\; dr'; \qquad \eta(\mathbf{r}) = 1 + \frac{\kappa(\mathbf{r})}{|\kappa_m(r)|}\,. \tag{8.3}$$

These relations generalise results obtained previously for projected surveys in 2D eqs. (2.1)–(2.2) and for tomographic bins in eqs. (2.4)–(2.5). The 3D reduced convergence $\eta(\mathbf{r})$ generalises the tomographic reduced convergence in eq. (7.3). Notice that tomographic weight $\omega_{(i)}(r)$ is replaced with $\omega(r, r')$ and tomographic $\kappa_{\rm min}^{(i)}$ is replaced with a radial function $\kappa_m(r)$.

8.1 3D one-point moments and PDF

We start with normalised moments of 3D convergence field $\kappa(\mathbf{r})$ which are now functions of radial coordinate r and are defined as follows:

$$S_p^\kappa(r) = \frac{\langle \kappa^p(\mathbf{r})\rangle_c}{\langle \kappa^2(\mathbf{r})\rangle_c^{p-1}}\,; \qquad \Phi_{1+\kappa}(r) = y + \sum_{p=2}^{\infty} \frac{S_p^\kappa(r)}{p!} y^p\,. \tag{8.4}$$

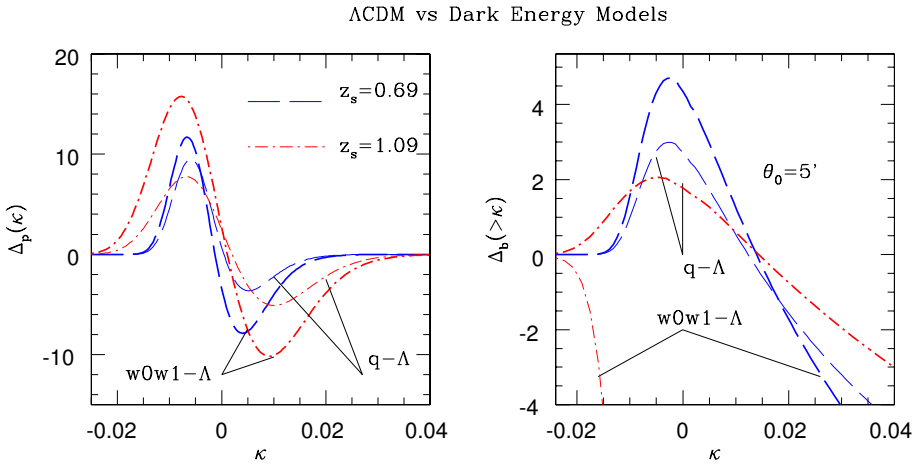

Figure 6. We compare the PDF and cumulative bias associated with tomographic convergence maps for various tomographic bins for two different dark energy models against the ΛCDM model. The left panel plots $\Delta_p(\kappa) = p(\kappa) - p_{\Lambda\rm CDM}(\kappa)$ for a smoothing angular scale of $\theta_0 = 5'$. The right panel depicts $\Delta_b^{(i)}(>\kappa) = b^{(i)}(>\kappa) - b^{(i)}_{\Lambda\rm CDM}(>\kappa)$ for the cumulative bias. Two different redshift bins are displayed $z_s = 0.698, 1.095$. For a given smoothing angular scale and a fixed redshift, the (thick) curves with higher positive peak heights correspond to the model $w_0 = -1, w_1 = 1$ and the (thin) ones with lower peak heights correspond to $w_0 = -0.9$, $w_1 = 0$.

Assuming an isotropic background Universe, the 3D mormalised moments $S_p^\kappa(r)$ and their generating function $\Phi_{1+\kappa}(r)$ becomes a function of r. The lower-order moments $\langle\kappa^p(\mathbf{r})\rangle_c$ for the 3D convergence maps $\langle\kappa^p(\mathbf{r})\rangle_c$ are expressed as a function of the multi-spectra B_p of the underlying density contrast $\delta(\mathbf{r})$:

$$\langle\kappa^p(\mathbf{r})\rangle_c \equiv \int_0^r dr' \, \frac{w_{3\rm D}^p(r,r')}{[d_A(r')]^{2(p-1)}} \int \frac{d^2\mathbf{l}_1}{(2\pi)^2} \cdots \int \frac{d^2\mathbf{l}_p}{(2\pi)^2} \mathrm{B}_p\left(\frac{\ell_1}{d_A(r')}, \cdots, \frac{\ell_p}{d_A(r')}; r'\right). \tag{8.5}$$

Using the *minimal model* of HA introduced in section 4 one can express $\Phi_{1+\kappa}(y;r)$ in terms of $\phi(y)$:

$$\Phi_\eta(y;r) = \frac{1}{\kappa_m(r)} \int_0^r dr' \left[\frac{d_A^2(r')}{\kappa_m(r')} \frac{\bar{\xi}_2^\kappa(r')}{\mathcal{J}_{\theta_0}(r')}\right] \phi\left[\omega_{3\rm D}(r',r) \frac{\kappa_m(r)}{d_A^2(r')} \frac{\mathcal{J}_{\theta_0}(r')}{\bar{\xi}_2^\kappa(r')} y\right]. \tag{8.6}$$

The corresponding tomographic relation is given in eq. (7.4). We can now extend eq. (7.5) and eq. (7.6) by introducing a parametric index r in the scaling function $h_\eta(x\,;r)$:

$$h_\eta(x\,;r) = \frac{1}{[\kappa_m(r)]} \int_0^r dr \left[\frac{\bar{\xi}_2^\kappa(r')}{\omega_{3\rm D}(r,r')\mathcal{J}_{\theta_0}(r')\kappa_m(r')}\right]^2 h\left(\frac{\bar{\xi}_2^\kappa(r')\, x}{\omega_{3\rm D}(r,r')\mathcal{J}_{\theta_0}(r')\kappa_m(r')}\right). \tag{8.7}$$

Using similar set of approximations we can now generalise the tomographic relationship in eq. (7.7) to following 3D relationship:

$$p(\kappa\,;r) = p_\eta(\eta(r))/|\kappa_m(r)| \tag{8.8}$$

Thus the discrete index in tomography is now replaced by the continuous radial distance r. Finally following the same logic we have the 3D normalised moments $S_p^\kappa(r) \approx S_p^\eta/|\kappa_m(r)|^{p-2}$; thus separating the effect of dynamics and background cosmology. Notice, that the PDF $p(\kappa;r)$ has only an *implicit* dependence on the radial coordinate r through $\kappa_m(r)$ and $\bar{\xi}_2^\kappa(r) = \langle\kappa^2(\mathbf{r})\rangle$. The final result obtained is independent of specific assumptions of a specific model of HA and indicates its more general applicability.

JCAP04(2014)004

8.2 3D two-point moments and bias

Extending the two-point tomographic cumulant-correlators $C_{pq}^{(ij)}$ in eq. (7.8) the 3D normalised cumulant correlators $C_{pq}^{\kappa}(r_1, r_2)$ can be expressed as follows:

$$C_{pq}^{\kappa}(r_1, r_2) = \frac{\langle \kappa_1^p \kappa_2^q \rangle_c}{[\langle \kappa_1^2 \rangle_c]^{p-1} [\langle \kappa_2^2 \rangle_c]^{q-1} \langle \kappa_1 \kappa_2 \rangle_c} \,. \tag{8.9}$$

We have introduced the shorthand notation $\kappa_1 = \kappa(\mathbf{r}_1)$ and $\kappa_2 = \kappa(\mathbf{r}_2)$ the cumulant correlator can be expressed interms of the multispectrum B_{p+q} as follwos:

$$\begin{aligned} \langle \kappa_1^p \kappa_2^q \rangle_c \equiv & \int_0^{r_0} dr' \frac{w_{3\mathrm{D}}^p(r_1, r')}{[d_A(r')]^{2(p-1)}} \frac{w_{3\mathrm{D}}^q(r_2, r')}{[d_A(r')]^{2(q-1)}} \\ & \times \int \frac{d^2\mathbf{l}_1}{(2\pi)^2} \cdots \int \frac{d^2\mathbf{l}_{p+q}}{(2\pi)^2} \, \mathrm{B}_{p+q} \left(\frac{\ell_1}{d_A(r')}, \cdots, \frac{\ell_{p+q}}{d_A(r')}; r' \right) . \end{aligned} \tag{8.10}$$

Here $r_0 = \min\{r_1, r_2\}$. The generating function $\beta_\eta(y_1, y_2; r_1, r_2)$ can be decompsed in two to independent generating functions $\beta_\eta(y_1; r_1)$. See eq. (7.8) for corresponding tomographic functions are $\beta^{(ij)}(y_1, y_2)$ and $\beta^{(i)}(y)$:

$$\begin{aligned} \beta_\eta(y_1, y_2; r_1, r_2) &= \sum_{p,q}^{\infty} \frac{C_{pq}^{\eta}(r_1, r_2)}{p!q!} y_1^p y_2^q = \sum_{p}^{\infty} \frac{C_{p1}^{\eta}(r_1)}{p!} y_1^p \sum_{q}^{\infty} \frac{C_{q1}^{\eta}(r_2)}{q!} y_2^q \\ &= \beta_\eta(y_1; r_1) \beta_\eta(y_2; r_2) \,. \end{aligned} \tag{8.11}$$

Where $\xi_2^{\kappa}(r_1, r_2) \equiv \langle \kappa_1 \kappa_2 \rangle$. The corresponding tomographic relations are given in eq. (7.9). Using these expression we can write:

$$\begin{aligned} \beta_\kappa(y_1, y_2; r_1, r_2) = & \int_0^{r_0} dr \, \frac{d_A(r)}{[\kappa_m(r_1)]} \frac{d_A(r)}{[\kappa_m(r_2)]} \frac{\mathcal{J}_{\theta_{12}}(r)}{\bar{\xi}_{12}^{\kappa}(r_1, r_2)} \frac{\bar{\xi}(r_1)}{\mathcal{J}_{\theta_0}(r)} \frac{\bar{\xi}(r_2)}{\mathcal{J}_{\theta_0}(r)} \\ & \times \beta_\eta \left(\frac{y_1}{\bar{\xi}^{\kappa}(r_1)} \frac{\omega_{3\mathrm{D}}(r, r_1)}{d_A^2(r)} \frac{\mathcal{J}_{\theta_0}(r)}{|\kappa_m(r_1)|} \right) \beta_\eta \left(\frac{y_2}{\bar{\xi}_2^{\kappa}(r_2)} \frac{\omega_{3\mathrm{D}}(r, r_2)}{d_A^2(r)} \frac{\mathcal{J}_{\theta_0}(r)}{|\kappa_m(r_2)|} \right) . \end{aligned} \tag{8.12}$$

Generalising the corresponding tomographic relation given in eq. (7.10), the two-point PDF in 3D can be expressed using the following relation:

$$p(\kappa_1, \kappa_2; r_1, r_2) = p(\kappa_1; r_1) p(\kappa_2; r_2) (1 + b(\kappa_1; r_1) \xi_{12}^{\kappa}(r_1, r_2) b(\kappa_2; r_2)) \,. \tag{8.13}$$

The 3D bias $b(\kappa; r)$ is related to the generating function $\tau(y; r) = \beta(y; r)$ by the following relation:

$$b_\eta(x; r) h_\eta(x; r) = -\frac{1}{2\pi i} \int_{-i\infty}^{+i\infty} dy \, \tau(y; r) \, \exp(xy) \,. \tag{8.14}$$

The corresponding tomographic relation is eq. (7.13). Finally, the corresponding 3D bias for the convergence field $b(\kappa; r)$ can be related following similar steps:

$$b(\kappa; r) = b_\eta(\eta(r)) / |\kappa_m(r)| \,. \tag{8.15}$$

As was the case with pdf $p(\kappa; r)$ the bias $b(\kappa; r)$ is not an implict function of radial coordiante r.

To incorporate the photometric redshift error, we have to convolve the posterior probability distribution $p_h(z'|z_h)$ with $w_{3\mathrm{D}}(r_1, r_2)$ using the procedure outlined in tomographic analysis.

JCAP04(2014)004

9 Effect of noise on one- and two-point PDF

The PDF we have considered so far are free from noise. In this section we will present the results of estimates of error relating to the PDFs, those at the level of one-point and two-point PDFs. These results will generalise the ones found by [36] for lower order moments and later by [52]. Inclusion of noise can be incorporated through a convolution. We will assume the noise to be Gaussian and uncorrelated with the signal. However the variance of the noise will depend on the surface density of galaxies in individual bins. With these simplifying assumption, for the i-th tomographic bin we can write:

$$p_n^{(i)}(\kappa) = \int_{-\infty}^{\infty} p^{(i)}(\kappa - n)\, p_G^{(i)}(n)\, dn\,. \tag{9.1}$$

Here $p_G^{(i)}(n)$ is the noise PDF assumed Gaussian, and $p_n^{(i)}(\kappa)$ is the convergence PDF in the presence of noise (the subscript G denotes Gaussian). We take $\sigma_\kappa^2 = \sigma_\epsilon^2/(2n_g\pi\theta_0^2)$. Here σ_ϵ is intrinsic ellipticity distribution of galaxies and n_g is the number denisty of galaxies and θ_0 is the smoothing angular scale. The two-point PDF can also be modified to include the effect of noise in a similar manner. The equivalent expression for 2PDF can be written as:

$$p_n^{(ij)}(\kappa_1, \kappa_2) = p_n^{(i)}(\kappa_1) p_n^{(j)}(\kappa_2)(1 + b_n^{(i)}(\kappa_1)\xi_{12}^{ij} b_n^{(j)}(\kappa_2))\,, \tag{9.2}$$

Which is obtained by convolving the noise PDF with the 2PDF:

$$p_n^{(ij)}(\kappa_1, \kappa_2) = \int_{-\infty}^{\infty} p^{(ij)}(\kappa_1 - n_1, \kappa_2 - n_2)\, p_G^{(i)}(n_1)\, p_G^{(j)}(n_2)\, dn_1\, dn_2\,. \tag{9.3}$$

Comparing eq. (9.2) and eq. (9.3) we can write the expression for the noisy bias $b_n(\kappa)$ as:

$$b_n^{(i)}(\kappa) = \int_{-\infty}^{\infty} p^{(i)}(\kappa - n) b^{(i)}(\kappa - n) p_G^{(i)}(n) dn \Big/ \int_{-\infty}^{\infty} p^{(i)}(\kappa - n) p_G^{(i)}(n)\, dn\,. \tag{9.4}$$

Notice that depending on redshift distribution of sources, the noise maps $n^{(i)}$ and $n^{(j)}$ can be different for two tomographic bins. We also assumed that noise in different bins are statistically independent. The cumulative bias for the i-th tomographic bin that include noise $b_n^{(i)}(> \kappa)$ can be expressed in terms of $p_n^{(i)}(\kappa)$ $b_n^{(i)}(\kappa)$ just as its noise-free counterpart:

$$b_n^{(i)}(> \kappa) = \int_{\kappa}^{\infty} p_n^{(i)}(\kappa) b_n^{(i)}(\kappa) d\kappa \Big/ \int_{\kappa}^{\infty} p_n^{(i)}(\kappa) d\kappa\,. \tag{9.5}$$

Errors associated with binned tomographic noisy PDF can be analysed using following quantites:

$$\mathrm{N} = n_g \pi \theta_0^2 = 314 \left(\frac{n_g}{100\ \mathrm{arcmin}^{-2}}\right) \left(\frac{\theta_0}{1\ \mathrm{arcmin}}\right)^2 \tag{9.6}$$

Here n_g is the number density of galaxies, θ_s is the smoothing angular scale in arc-minutes for a given survey strategy. For a given survey we denote the area covered by A and introduce a parameter N_c which will be used in expressing the signal-to-noise estimates of the PDF $p(\kappa)$. We define the following variable that will be useful in qunatifying scatter in a noisy PDF:

$$\mathrm{N}_c = \frac{A}{(2\theta_0)^2} = 2.7 \times 10^4 \left(\frac{A}{300\ \mathrm{degree}^2}\right) \left(\frac{\theta_0}{1\ \mathrm{arcmin}}\right)^{-2}. \tag{9.7}$$

JCAP04(2014)004

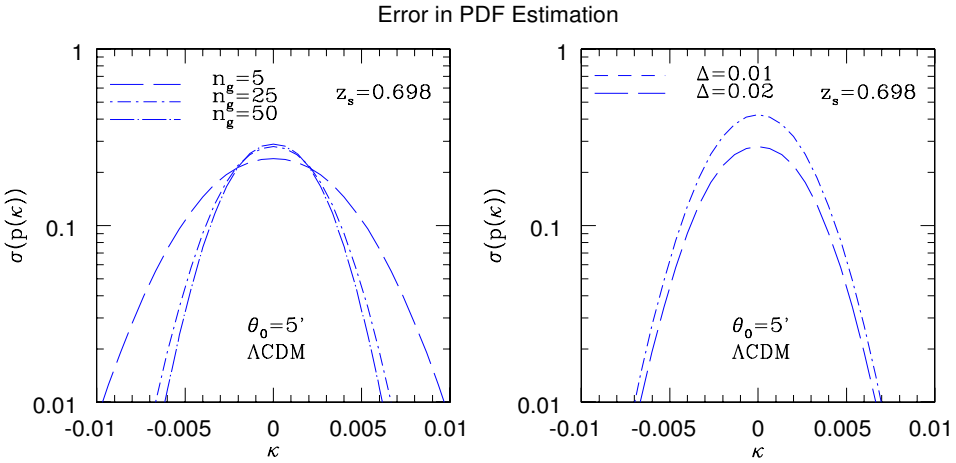

Figure 7. The sacatter in estimation of binned PDF for a given intrinsic ellipticity distribution and sky coverage is displayed. We assume an all-sky coverage. The effect of intrinsic ellipticity distribution is displayed in the left panel. The right panel depicts the effect of binning. The angular scale in each case is $\theta_0 = 5'$ and the redshift is $z_s = 0.698$. The expression for $\sigma(p(\kappa))$ is given in eq. (9.8). For the left panel we consider $\Delta = 0.02$ and for the right panel $n_g = 25$. A background ΛCDM cosmology is accumed for these calculations.

Finally the scatter $\sigma(p(\kappa))$ in the measured convergence power sepctra $p(\kappa)$ can be expressed as [52]:

$$\frac{\sigma\left(p_n^{(i)}(\kappa)\right)}{p_n^{(i)}(\kappa)} = \left[\frac{1}{\mathrm{N}_c}\left(\frac{1}{2p_n^{(i)}(\kappa)\Delta} - 1\right)\right]^{1/2} \tag{9.8}$$

These expression can be modified and used to compute the scatter in individual redshift bins by simply changing $\bar{n}_g$ to surface density of individual bins $\bar{n}_g^{(i)}$ and $p(\kappa)$ to $p^{(i)}(\kappa)$. The source density for individual bins for a given survey can be computed using $\bar{n}^{(i)} = \int_{z_i}^{z_{i+1}} p_s(z)dz$. The bin width Δ is left as a free parameter. In figure 7 we have plotted the scatter $\sigma(p_n^{(i)}(\kappa)$ as a function of intrinsic ellipticity distribution and bin width for a smoothing angular scale of $\theta_0 = 5'$ and redshift $z_s = 0.698$. The results for the difference in noisy PDFs are plotted in figure 8.

We find that the w0w1 model considered by us shows greater departure fromthe ΛCDM model compared to qCDM model. We find that the departure increases with redshift z. The peak is in both dark energy models is shifted to lower values of κ and the long κ tail is less pronounced compared to the ΛCDM model.

10 Conclusions

The statistics of weak lensing convergence κ is studied using tomography as well as in 3D. The PDFs for the individual bins are constructed by generalization of the previously introduced global variable for projected surveys $\kappa^{\min}$. This is achieved by introducing $\kappa_{(i)}^{\min}$ for each individual bins. Next, using $\kappa_{(i)}^{\min}$, reduced variable $\eta^{(i)}$ is defined for individual bins whose statistics can directly be linked to that of underlying density contrast δ. The convergence in individual bins can then be mapped to unique values of $\eta = 1 + \delta$ for a given smoothing angular scales θ_0. Similar results were also obtained for 3D surveys where we generalise $\kappa_{(i)}^{\min}$ to a radial function i.e. $\kappa(r)$.

JCAP04(2014)004

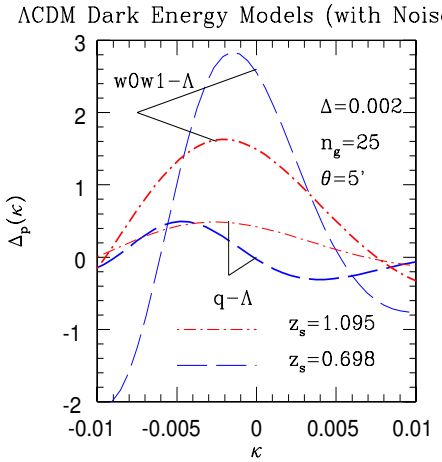

Figure 8. The difference of noisy ΛCDM PDF and dark energy models $\Delta_p(\kappa) = p(\kappa) - p_{\Lambda\mathrm{CDM}}(\kappa)$ is plotted as a function of κ. The smoothing angular scale, bin size and galaxy number density is as depicted. The scatter in estimation is smaller compared to the difference in the PDFs considered. The comsological parameters considered are the same as the ones in figure 6. The two survey configurations that we have considered both produces near identical results.

For modelling the statistics of underlying density contrast δ we have assumed two completely different model: the HA along with its perturbative counterpart as well as the lognormal distribution. Both these approximations have been used successfully in various cosmological contexts before. There are a wide class of models that are available under the general category of HA. The main motivation behind our choice of a specific hierarchy is simplicity.

In agreement with [30], we find that the dynamical and geometrical contributions can be treated separately. The reduced convergence in 2D is independent of the background geometry of the universe and essentially probe the evolution of gravitational clustering. Here we showed that a set of $\kappa^{\mathrm{min}}_{(i)}$, defined for a given set of redshift slices, are adequate to characterize not only individual PDFs for each bin but are also sufficient to study the joint two-point PDF among two different bins. Similarly in 3D $\kappa_m(r)$ encode the background dynamics and the reduced 3D convergence $\eta(r)$ is effectively determined by the gravitational dynamics.

In our analysis we have ignored the noise from intrinsic ellipticity distribution of galaxies as well as from shot noise resulting from finite number of galaxies that are used to trace the underlying mass distribution. These issues have been dealt with in great detail in [36, 53]. Dividing the source population into bins reduced the number-density of sources. This in turn will increase the level of noise or the scatter in the estimator. However, we have considered two different survey configurations, i.e. LSST and DES and found that for our choice of tomographic bins the one- and two-point PDFs are very similar in nature.

The lognormal distribution has already been used to model the statistics of weak lensing observables [33, 49] and the clustering of Lyman alpha absorption systems e.g. [11]. One-to-one mapping of initial density fields to evolved density fields using maps that are consistent with lognormal distribution function was not found to be very successful and the success of a lognormal distribution function in reproducing the statistics of gravitational clustering still remains somewhat unclear. We have used the lognormal distribution to characterise the topology of convergence maps in A.

Weak lensing surveys can be cross-correlated with external data sets including frequency cleaned maps of secondaries from ongoing CMB surveys; e.g. the thermal Sunyaev-Zeldovic

JCAP04(2014)004

(tSZ) maps or y-maps that are available from CMB surveys such as Planck. The cross-correlation with tomographic or 3D convergence can help to understand the evolution of cosmological pressure fluctuations responsible for tSZ effect with redshift.

Acknowledgments

DM and PC acknowledges support from STFC standard grant ST/G002231/1 at School of Physics and Astronomy at Cardiff University where this work was initiated. The work was completed at University of Sussex where DM was supported by a STFC grant. We would like to thank Alan Heavens, Patrick Valageas, Ludo van Waerbeke and Sanaz Vafei for many useful discussions. The numerical results were obtained using a modified version of a code made available to us for computing the PDF and bias by Francis Bernardeau.

A Tomographic topography and lognormal approximation

In the text of the paper we have obtained generic results for the PDFs and their lower order moments. These results are complemetary to studies involving morphological statistics as they are affected by different set of systematics (see e.g. [29] and references there in for a recent discussion in the context of weak lensing). Morphological studies involve toplogical descriptors that can be used to study the toplogies of contours are known as Minkowski functionals (MF) [46].

The explicit expression of the MFs are given in terms of the threshold $\nu_{(i)} = \kappa_{(i)}/\langle\kappa^2_{(i)}\rangle_c^{1/2}$ in the i-th tomographic bin.

$$v_0^{(i)}\left(\nu_{(i)}\right) = \langle\Theta\left(\kappa_{(i)} - \nu_{(i)}\langle\kappa^2_{(i)}\rangle_c^{1/2}\right)\rangle_c\,; \tag{A.1}$$

$$v_1^{(i)}\left(\nu_{(i)}\right) = \frac{\pi}{8}N_1\left(\nu_{(i)}\right) = \frac{\pi}{8}\langle\delta_D\left(\kappa_{(i)} - \langle[\kappa_{(i)}]^2\rangle^{1/2}\nu_{(i)}\right)|\nabla\kappa_{(i)}|\rangle \tag{A.2}$$

$$v_2^{(i)}\left(\nu_{(i)}\right) = G_2\left(\nu\right) = \langle\delta_D\left(\kappa_{(i)} - \langle[\kappa_{(i)}]^2\rangle_c^{1/2}\nu_{(i)}\right)\rangle_c \tag{A.3}$$

Here Θ denotes heaviside step function. The functions $N_1(\nu)$ and $G_2(\nu)$ are level crossing statistics and Genus statistics. The higher order MFs rely on higher order derivative terms and contained independent information. The MFs can be evaluated from the lognormal PDF [49] which has the following approximate form:

$$v^{(i)}_{0,\ln}(\nu_{(i)}) = \frac{1}{2}\mathrm{erfc}\left(\frac{y_{(i)}(\nu_{(i)})}{\sqrt{2}}\right); \tag{A.4}$$

$$v^{(i)}_{1,\ln}(\nu_{(i)}) = \frac{1}{8\sqrt{2}}\frac{1}{\sqrt{|\kappa^{\min}_{(i)}|^2 + \langle\kappa^2_{(i)}\rangle_c}}\frac{\langle\left(\nabla\kappa_{(i)}\right)^2\rangle}{[\sigma^{(i)}_{ln}]}\exp\left(-\frac{y^2_{(i)}(\nu_{(i)})}{2}\right); \tag{A.5}$$

$$v^{(i)}_{2,\ln}(\nu_{(i)}) = \frac{1}{2(2\pi)^{3/2}}\frac{1}{\sqrt{|\kappa^{\min}_{(i)}|^2 + \langle\kappa^2_{(i)}\rangle_c}}\frac{\langle\left(\nabla\kappa_{(i)}\right)^2\rangle}{[\sigma^{(i)}_{ln}]^2}\exp\left(-\frac{y^2_{(i)}(\nu_{(i)})}{2}\right). \tag{A.6}$$

Where we have introduced the following notation:

$$y_{(i)}(\nu_{(i)}) \equiv \frac{\Sigma^{(i)}_{\ln}}{2} + \frac{\ln\left(1 + \nu_{(i)}\langle\kappa^2_{(i)}\rangle_c^{1/2}\Big/|\kappa^{\min}_{(i)}|\right)}{\sigma^{(i)}_{ln}}; \tag{A.7}$$

$$[\Sigma^{(i)}_{\ln}]^2 = \ln\left(1 + \frac{\langle\kappa^2_{(i)}\rangle_c}{|\kappa^{\min}_{(i)}|^2}\right) \tag{A.8}$$

JCAP04(2014)004

The corresponding 3D expressions can be derived by replacing $\nu_{(i)}$ with $\nu(r)=\kappa(r)/\langle\kappa^2(r)\rangle_c^{1/2}$ and $\kappa_{(i)}^{\min}$ with $\kappa_m(r)$ in eqs. (A.4)–(A.8). A detailed study will be presented elsewhere.

References

[1] L. Amendola and S. Tsujikawa, *Dark Energy: Theory and Observations*, Cambridge University Press (2010) [ISBN-10: 0521516005].

[2] R. Balian and R. Schaeffer, *Scale-invariant matter distribution in the universe. I - Counts in cells*, *Astron. Astrophys.* **220** (1989) 1.

[3] D.J. Bacon, A.R. Refregier and R.S. Ellis, *Detection of weak gravitational lensing by large-scale structure*, *Mon. Not. Roy. Astron. Soc.* **318** (2000) 625 [astro-ph/0003008] [INSPIRE].

[4] F. Bernardeau, S. Colombi, E. Gaztanaga and R. Scoccimarro, *Large scale structure of the universe and cosmological perturbation theory*, *Phys. Rept.* **367** (2002) 1 [astro-ph/0112551] [INSPIRE].

[5] F. Bernardeau and R. Schaeffer, *Galaxy correlations, matter correlations and biasing*, *Astron. Astrophys.* **255** (1992) 1.

[6] F. Bernardeau, *The Gravity induced quasi-Gaussian correlation hierarchy*, *Astrophys. J.* **392** (1992) 1 [INSPIRE].

[7] F. Bernardeau, *The Effects of smoothing on the statistical properties of large scale cosmic fields*, *Astron. Astrophys.* **291** (1994) 697 [astro-ph/9403020] [INSPIRE].

[8] F. Bernardeau and L. Kofman, *Properties of the cosmological density distribution function*, *Astrophys. J.* **443** (1995) 479 [astro-ph/9403028] [INSPIRE].

[9] F. Bernardeau and R. Schaeffer, *Halo correlations in nonlinear cosmic density fields*, *Astron. Astrophys.* **349** (1999) 697 [astro-ph/9903387] [INSPIRE].

[10] F. Bernardeau and P. Valageas, *Construction of the one-point pdf of the local aperture mass in weak lensing maps*, *Astron. Astrophys.* **364** (2000) 1 [astro-ph/0006270] [INSPIRE].

[11] H.G. Bi and A.F. Davidsen, *Evolution of structure in the intergalactic medium and the nature of the Lyα forest*, *Astrophys. J.* **479** (1997) 523 [astro-ph/9611062] [INSPIRE].

[12] F.R. Bouchet, M.A. Strauss, M. Davis, K.B. Fisher, A. Yahil and J.P. Huchra, *Moments of the Counts Distribution in the 1.2 Jansky IRAS Galaxy Redshift Survey*, *Astrophys. J.* **417** (1993) 36 [astro-ph/9305018] [INSPIRE].

[13] P.G. Castro, A.F. Heavens and T.D. Kitching, *Weak lensing analysis in three dimensions*, *Phys. Rev.* **D 72** (2005) 023516 [astro-ph/0503479] [INSPIRE].

[14] J. Carron and M.C. Neyrinck, *On the inadequacy of N-point correlation functions to describe nonlinear cosmological fields: explicit examples and connection to simulations*, *Astrophys. J.* **750** (2012) 28 [arXiv:1201.1444] [INSPIRE].

[15] P. Coles and B. Jones, *A Lognormal model for the cosmological mass distribution*, *Mon. Not. Roy. Astron. Soc.* **248** (1991) 1 [INSPIRE].

[16] S. Colombi, *A 'Skewed' lognormal approximation to the probability distribution function of the large scale density field*, *Astrophys. J.* **435** (1994) L536 [astro-ph/9402071] [INSPIRE].

[17] S. Colombi, F. Bernardeau, F.R. Bouchet and L. Hernquist, *Extended perturbation theory for the local density distribution function*, *Mon. Not. Roy. Astron. Soc.* **287** (1997) 241 [astro-ph/9610253] [INSPIRE].

[18] S. Das and J.P. Ostriker, *Testing a new analytic model for gravitational lensing probabilities*, *Astrophys. J.* **645** (2006) 1 [astro-ph/0512644] [INSPIRE].

[19] B. Joachimi and A.N. Taylor, *Forecasts of non-Gaussian parameter spaces using Box-Cox transformations*, *Mon. Not. Roy. Astron. Soc.* **416** (2011) 1010 [arXiv:1103.3370] [INSPIRE].

JCAP04(2014)004

[20] A. Heavens, *3D weak lensing*, *Mon. Not. Roy. Astron. Soc.* **343** (2003) 1327 [astro-ph/0304151] [INSPIRE].

[21] S. Hilbert, J. Hartlap and P. Schneider, *Cosmic-shear covariance: The log-normal approximation*, *Astron. Astrophys.* **536** (2011) A85 [arXiv:1105.3980] [INSPIRE].

[22] B. Jain, U. Seljak and S.D.M. White, *Ray tracing simulations of weak lensing by large scale structure*, *Astrophys. J.* **530** (2000) 547 [astro-ph/9901191] [INSPIRE].

[23] N. Kaiser, *Weak gravitational lensing of distant galaxies*, *Astrophys. J.* **388** (1992) 272 [INSPIRE].

[24] N. Kaiser, G. Wilson and G.A. Luppino, *Large scale cosmic shear measurements*, astro-ph/0003338 [INSPIRE].

[25] I. Kayo, A. Taruya and Y. Suto, *Probability distribution function of cosmological density fluctuations from Gaussian initial condition: comparison of one- and two-point log-normal model predictions with N-body simulations*, *Astrophys. J.* **561** (2001) 22 [astro-ph/0105218] [INSPIRE].

[26] T.D. Kitching and A.F. Heavens and L. Miller, *3D Photometric Cosmic Shear*, *Mon. Not. Roy. Astron. Soc.* **413** (2011) 2923 [arXiv:1007.2953] [INSPIRE].

[27] L. Kofman, E. Bertschinger, J.M. Gelb, A. Nusser and A. Dekel, *Evolution of one point distributions from Gaussian initial fluctuations*, *Astrophys. J.* **420** (1994) 44 [astro-ph/9311028] [INSPIRE].

[28] D.N. Limber, *The Analysis of Counts of the Extragalactic Nebulae in Terms of a Fluctuating Density Field. II*, *Astrophys. J.* **119** (1954) 665 [INSPIRE].

[29] D. Munshi, L. van Waerbeke, J. Smidt and P. Coles, *From Weak Lensing to non-Gaussianity via Minkowski Functionals*, *Mon. Not. Roy. Astron. Soc.* **419** (2012) 536 [arXiv:1103.1876] [INSPIRE].

[30] D. Munshi and B. Jain, *The statistics of weak lensing at small angular scales: probability distribution function*, *Mon. Not. Roy. Astron. Soc.* **318** (2000) 109 [astro-ph/9911502] [INSPIRE].

[31] D. Munshi and B. Jain, *Statistics of weak lensing at small angular scales: analytical predictions for lower order moments*, *Mon. Not. Roy. Astron. Soc.* **322** (2001) 107 [astro-ph/9912330] [INSPIRE].

[32] D. Munshi, P. Valageas, L. Van Waerbeke and A. Heavens, *Cosmology with Weak Lensing Surveys*, *Phys. Rept.* **462** (2008) 67 [astro-ph/0612667] [INSPIRE].

[33] D. Munshi, *Probing the gravity induced bias with weak lensing: test of analytical results against simulations*, *Mon. Not. Roy. Astron. Soc.* **318** (2000) 145 [astro-ph/0001240] [INSPIRE].

[34] D. Munshi adn P. Coles, *Weak lensing from strong clustering*, *Mon. Not. Roy. Astron. Soc.* **313** (2000) 148.

[35] D. Munshi and P. Coles, *Cosmic statistics through weak lenses*, *Mon. Not. Roy. Astron. Soc.* **329** (2002) 797 [astro-ph/0003354] [INSPIRE].

[36] D. Munshi and P. Coles, *Error estimates for measurements of cosmic shear*, *Mon. Not. Roy. Astron. Soc.* **338** (2003) 846 [astro-ph/0003481] [INSPIRE].

[37] D. Munshi, P. Coles and A.L. Melott, *From snakes to stars, the statistics of collapsed objects — I. lower-order clustering properties*, *Mon. Not. Roy. Astron. Soc.* **307** (1999) 387 [astro-ph/9812337] [INSPIRE].

[38] D. Munshi, P. Coles and A.L. Melott, *From snakes to stars, the statistics of collapsed objects. 2. Testing a generic scaling ansatz for hierarchical clustering*, *Mon. Not. Roy. Astron. Soc.* **310** (1999) 892 [astro-ph/9902215] [INSPIRE].

[39] D. Munshi, A.L. Melott and P. Coles, *Generalized Cumulant Correlators and Hierarchal Clustering*, *Mon. Not. Roy. Astron. Soc.* (1999) **311** 149.

JCAP04(2014)004

[40] D. Munshi and P. Valageas, *Evolution of the Cosmological Density Distribution Function: A New Analytical Model*, *Mon. Not. Roy. Astron. Soc.* **354** (2004) 1146.

[41] D. Munshi, P. Valageas and A.J. Barber, *Weak lensing shear and aperture-mass from linear to non-linear scales*, *Mon. Not. Roy. Astron. Soc.* **350** (2004) 77 [astro-ph/0309698] [INSPIRE].

[42] D. Munshi, A. Heavens and P. Coles, *Higher-order Convergence Statistics for Three-dimensional Weak Gravitational Lensing*, *Mon. Not. Roy. Astron. Soc.* **411** (2011) 2161 [arXiv:1002.2089] [INSPIRE].

[43] D. Munshi, T. Kitching, A. Heavens and P. Coles, *Higher Order Statistics for Three-dimensional Shear and Flexion*, *Mon. Not. Roy. Astron. Soc.* **416** (2011) 629 [arXiv:1012.3658] [INSPIRE].

[44] D. Munshi and Y. Wang, *How sensitive are weak lensing statistics to dark energy content?*, *Astrophys. J.* **583** (2003) 566 [astro-ph/0206483] [INSPIRE].

[45] P.J.E. Pebles, *The Large Scale Structure of the Universe*, Princeton University Press (1980).

[46] J. Schmalzing and T. Buchert, *Beyond genus statistics: A Unifying approach to the morphology of cosmic structure*, *Astrophys. J.* **482** (1997) L1 [astro-ph/9702130] [INSPIRE].

[47] I. Szapudi and A.S. Szalay, *Higher order statistics of the galaxy distribution using generating functions*, *Astrophys. J.* **408** (1993) 43.

[48] I. Szapudi and A.S. Szalay, *Cumulant correlators from the APM*, *Astrophys. J.* **481** (1997) L1 [*Erratum ibid.* **515** (1999) L43] [astro-ph/9702015] [INSPIRE].

[49] A. Taruya, M. Takada, T. Hamana, I. Kayo and T. Futamase, *Lognormal property of weak-lensing fields*, *Astrophys. J.* **571** (2002) 638 [astro-ph/0202090] [INSPIRE].

[50] R. Takahashi, M. Oguri, M. Sato and T. Hamana, *Probability Distribution Functions of Cosmological Lensing: Convergence, Shear and Magnification*, *Astrophys. J.* **742** (2011) 15 [arXiv:1106.3823] [INSPIRE].

[51] L. van Waerbeke et al., *Detection of correlated galaxy ellipticities on CFHT data: First evidence for gravitational lensing by large scale structures*, *Astron. Astrophys.* **358** (2000) 30 [astro-ph/0002500] [INSPIRE].

[52] P. Valageas, D. Munshi and A.J. Barber, *On estimation of non-Gaussianities from weak lensing surveys*, *Mon. Not. Roy. Astron. Soc.* **356** (2005) 386 [astro-ph/0402227] [INSPIRE].

[53] P. Valageas, A.J. Barber and D. Munshi, *Analytical predictions for statistics of cosmic shear: Tests against simulations*, *Mon. Not. Roy. Astron. Soc.* **347** (2004) 654 [astro-ph/0303472] [INSPIRE].

[54] P. Valageas, *Statistical properties of the convergence due to weak gravitational lensing by nonlinear structures*, *Astron. Astrophys.* **356** (2000) 771 [astro-ph/9911336] [INSPIRE].

[55] Y. Wang, *Dark Energy*, Wiley-VCH (2010) [ISBN-10: 9783527409419].

[56] S.D.M. White, *The hierarchy of correlation functions and its relation to other measures of galaxy clustering*, *Mon. Not. Roy. Astron. Soc.* **186** (1979) 145 [INSPIRE].

[57] Y. Wang and P.M. Garnavich, *Measuring time dependence of dark energy density from type Ia supernova data*, *Astrophys. J.* **552** (2001) 445 [astro-ph/0101040] [INSPIRE].

[58] D.M. Wittman, J.A. Tyson, D. Kirkman, I. Dell'Antonio and G. Bernstein, *Detection of weak gravitational lensing distortions of distant galaxies by cosmic dark matter at large scales*, *Nature* **405** (2000) 143 [astro-ph/0003014] [INSPIRE].

[59] Y. Yu, P. Zhang, W. Lin, W. Cui and J.N. Fry, *Gaussianizing the non-Gaussian lensing convergence field I: the performance of the Gaussianization*, *Phys. Rev.* **D 84** (2011) 023523 [arXiv:1103.2858] [INSPIRE].

[60] Y. Yu, P. Zhang, W. Lin, W. Cui and J.N. Fry, *Gaussianizing the non-Gaussian lensing convergence field II: the applicability to noisy data*, *Phys. Rev.* **D 86** (2012) 023515 [arXiv:1201.4527] [INSPIRE].

JCAP04(2014)004